Applied Thermal Engineering 104 (2016) 203–211

Contents lists available at ScienceDirect

Applied Thermal Engineering

journal homepage: www.elsevier.com/locate/apthermeng

Research Paper

Numerical investigation of membrane based heat exchanger with partially blocked channels

S. Sabek [a,*], F. Tiss [a], R. Chouikh [b], A. Guizani [a]

[a] Thermal Process Laboratory Research and Technologies Center of Energy, Borj-Cedria Science and Technologies Park, BP 95, 2050 Hammam-lif, Tunisia
[b] King Khalid University, Faculty of Science, Physics Department, P.O. Box 9004, Abha 61413, Saudi Arabia

HIGHLIGHTS

- A partially blocked membrane based heat exchanger is numerically investigated.
- Impacts of two parameters ((*n*), (*r*)) on heat and mass distributions are evaluated.
- Impacts of air velocity on the fresh and exhaust air channels are established.
- Impacts of membrane proprieties on the Nusselt and Sherwood numbers are mentioned.
- Comparison between two flow arrangements is illustrated.

ARTICLE INFO

Article history:
Received 28 January 2016
Revised 13 April 2016
Accepted 28 April 2016
Available online 7 May 2016

Keywords:
Membrane based heat exchanger
Blocks
Effectiveness
Flow arrangements

ABSTRACT

Contrary to the traditional approach assuming the same parallel plate membrane based heat exchanger, a new proposition of exchanger design is investigated in this paper. The channels of membrane based heat exchanger are partially blocked by insertion of metal blocks. In order to evaluate their impacts on the heat and mass transfer distributions, a two-dimensional model including the momentum, heat and mass transport equations is solved by CFD code. Significant parameters such as obstacles number and form ratio are mentioned. The results show that the including of obstacles enhances the heat and mass transfer rates between the fresh and exhaust air channels. A low obstacles number leads to a large (small) air temperature and specific humidity ratio values in the exhaust (fresh) air channel. In addition, obstacle form ratio has a strong effect on the temperature and humidity distributions when it becomes higher. Also, this investigation takes into account the effect of membrane proprieties and flow arrangements which also have a strong effect on the heat and mass transfer rates.

1. Introduction

The Membrane Based Heat Exchangers (MBHEs) are not just significant equipments to provide a comfortable ambiance but also to control respiratory diseases [1]. Due to their high thermal conductivity, diffusion coefficient and homogenous pore distribution in comparison with other types of membranes, the modified Polyvinylalcohol (PVA) is one of the most used in the MBHEs [2,3]. In reality, the MBHEs operation involves simultaneous and complex processes such as fluid flow as well as heat and mass transfer [3]. It is obvious that one of the most important processes significantly influencing heat exchanger performances is the heat and mass transmission through the membrane. Therefore, design of the heat exchangers is a significant factor to improve the global system performance. During the last years, a lot of studies have been focused on the impact of the various flow arrangements such as co-current, counter-current and cross-flow [4,5].

In general, hydrophilic polymer membranes are characterized by their permeability only to the vapor and are applied in air dehumidification processes. Recent studies specify that the MBHE performance may be related to the membrane proprieties [6–8]. The permeability is a material parameter that describes the resistance to the humid air flow exhibited by the porous media. In literature, several materials have been investigated such as Nafion [9,10], cellulose triacetate [11], polyether-polyurethane [12], polyethersulfone [13,14], polyvinylidene fluoride [15], and polystyrene-sulfonate [16].

Mathematical modeling of mass and heat transfer mechanisms in the channels and within hydrophilic membrane is presented and then, numerical simulations are considered to obtain the operational status and to analyze mass and heat exchange in the MBHEs.

* Corresponding author.
E-mail address: seifennasr.sabek@gmail.com (S. Sabek).

http://dx.doi.org/10.1016/j.applthermaleng.2016.04.167
1359-4311/

Nomenclature

a	obstacle height (m)
b	obstacle width (m)
c	distance between two successive obstacles (m)
D_v	vapor diffusivity in the vapor-air mixture ($m^2\ s^{-1}$)
D_h	hydraulic diameter (m)
h	convective heat transfer coefficient ($W\ m^{-2}\ K^{-1}$)
H	channel height (m)
k	convective mass transfer coefficient ($m\ s^{-1}$)
Nu	Nusselt number ($Nu = \frac{hD_h}{\lambda_a}$)
P	pressure (Pa)
Pr	Prandtl number ($Pr = \frac{\nu}{\alpha}$)
Re	Reynolds number ($Re = \frac{u_0 D_h}{\nu}$)
Sc	Schmidt number ($Sc = \frac{\nu}{D_v}$)
Sh	Sherwood number ($Sh = \frac{kD_h}{D_v}$)
T	temperature (K)
u, v	velocity ($m\ s^{-1}$) for x and y directions respectively
u_0	mean velocity value ($m\ s^{-1}$)
x, y	coordinates (m)
x_f	channel length (m)
y_f	channel width (m)

Greek letters

α	thermal diffusivity ($m^2\ s^{-1}$)
ρ	air density ($kg\ m^{-3}$)
λ_a	air heat conductivity ($W\ m^{-1}\ K^{-1}$)
ν	kinematic viscosity ($m^2\ s^{-1}$)
δ	membrane thickness (μm)
τ_h	conductivity ratio $\left(\tau_h = \frac{\lambda_m}{\lambda_a}\right)$
τ_m	diffusivity ratio $\left(\tau_m = \frac{D_m}{D_v}\right)$
ω	humidity ratio ($kg\ kg^{-1}$)

Subscripts

ei	inlet exhaust air
fi	inlet fresh air
fo	outlet fresh air
m	membrane

A few numerical models for the heat exchanger and thermal management have been established in previous works. Min and Su [17] developed a mathematical model to analyze the heat and mass transfer in the MBHE core. Their results show that, as the moisture diffusivity in membrane increases with a constant sorption, the sensible effectiveness maintains almost unchanged. In a theoretical study, Min and Duan [18] analyzed the heat and mass transfer in total heat exchanger core and investigated his performance under various weather conditions. They concluded that the variation of the outdoor air humidity has a strong effect on the latent effectiveness when the heat and moisture transferred in either co-current or counter direction across membrane. Chung et al. [19] developed a numerical model to describe heat and mass transfer in a cross flow direct contact membrane distillation. Statistical analyses results showed a predominant feed flow rates and a smallest feed temperatures effects on mass transfer coefficients. Moghaddam et al. [20] studied numerically the steady state effectiveness of the small scale single panel liquid to air membrane energy exchanger. Their results showed that the latent and total effectiveness of the small scale liquid to air membrane energy exchanger are increased with reducing the membrane-vapor diffusion resistance, whereas the sensible effectiveness is unchanged.

Recently, Zhang [21] studied the heat and mass transfer in a quasi counter flow MBHE; their results showed that the quasi flow arrangement has better performance than cross flow due to the important heat and mass transfer caused by the counter flow zones. In consequence, the sensible and latent effectiveness are improved by 5%. Yu et al. [22] developed a numerical simulation of heat and mass transfer of laminar flow in a hollow fiber module for direct membrane distillation. They concluded that at the feed and permeate sides, the deviation of the membrane wall temperature from the fluid bulk phase leads to the temperature polarization effect which is decreased initially and then increased along the fiber length.

A comprehensive investigation of different air channel designs and their impacts on the thermal behaviors and moisture recovery in the MBHE is still important. This paper presents our attempts in this direction to investigate the effects of a few important operating parameters on the thermal management with newly MBHE design. The purpose is to develop the appropriate heat exchanger design under different conditions. Parametric study based on numerical simulation can be considered as an efficient method to attain our objective. The originality of our work is to insert metal blocks along the two channels and investigate their effects on the heat and mass transfer. This investigation is based on the partial blocks form ratio. The air flow channel has a tight, solid layer as a side-wall which their morphology may influence on the heat and mass transport from channel to the membrane surface and consequently, may affect the overall exchanger performance.

2. Mathematical formulation

In the proposed geometry, the Partially Blocked Membrane Based Heat Exchanger (PB MBHE) is similar to the simple MBHE developed by [23–26] with an addition of tetragon obstacles in solid layer configuration as shown in Fig. 1. The specific parameters of the PB MBHE are illustrated in Table 1.

The fresh and exhaust air streams in the PB MBHE are separated by hydrophilic membrane (modified PVA (poly-vinyl-alcohol)) that permits moisture transmission between two channels as shown in Fig. 1. The moisture transfers from highly to less humid air streams through the modified PVA membrane.

To solve the model of MBHE domain, a mathematical formulation is developed on the steady two-dimensional model. The following assumptions are made:

- The air flows in the MBHE are assumed to be laminar and incompressible.
- The membrane is isotropic and homogeneous porous medium.

The following equations governing the conservation of mass, momentum, energy, and vapor water concentration can be written as below:

The mass conservation equation of the air streams in channels is:

$$\frac{\partial \rho}{\partial t} = -\nabla \cdot (\rho \vec{V}) \tag{1}$$

Eq. (1) in two dimensional can be expressed as:

$$\frac{\partial u}{\partial x} + \frac{\partial v}{\partial y} = 0 \tag{2}$$

Conservation of momentum equations in 2D can be written as:

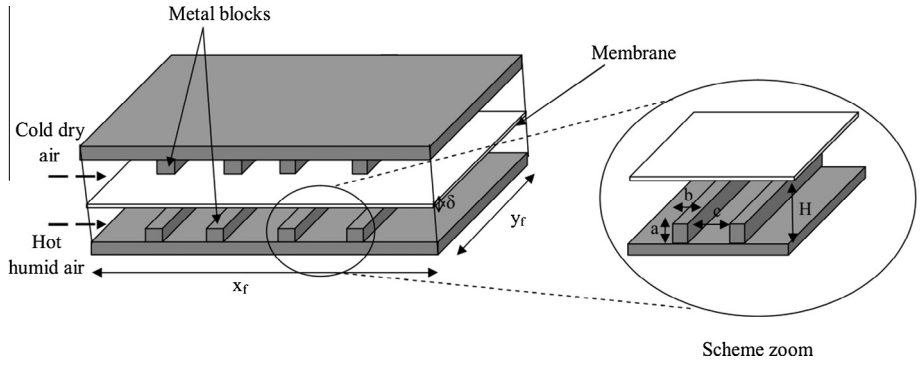

Fig. 1. Schematic description of the PB MBHE design.

Table 1
Specifications of the PB MBHE.

Parameters	Values	Unit
x_f	185	mm
y_f	185	mm
H	4	mm
δ	100	μm
λ_m	0.13	W m^{-1} K^{-1}
D_m	$8 \cdot 10^{-6}$	m^2 s^{-1}

$$u\frac{\partial u}{\partial x}+v\frac{\partial u}{\partial y}=-\frac{1}{\rho}\frac{\partial p}{\partial x}+\nu\left[\frac{\partial^2 u}{\partial x^2}+\frac{\partial^2 u}{\partial y^2}\right] \tag{3}$$

$$u\frac{\partial v}{\partial x}+v\frac{\partial v}{\partial y}=-\frac{1}{\rho}\frac{\partial p}{\partial y}+\nu\left[\frac{\partial^2 v}{\partial x^2}+\frac{\partial^2 v}{\partial y^2}\right] \tag{4}$$

In addition, heat transfer in the MBHE is modeled using the energy equation as expressed:

$$u\frac{\partial T}{\partial x}+v\frac{\partial T}{\partial y}=\alpha\left[\frac{\partial^2 T}{\partial x^2}+\frac{\partial^2 T}{\partial y^2}\right] \tag{5}$$

During moisture transfer process, water vapor molecules are transported through membrane by diffusion caused by water vapor concentration gradient between fresh and exhaust air channels [27]. The vapor water transport is governed as [28]:

$$u\frac{\partial \omega}{\partial x}+v\frac{\partial \omega}{\partial y}=D_v\left[\frac{\partial^2 \omega}{\partial x^2}+\frac{\partial^2 \omega}{\partial y^2}\right] \tag{6}$$

Further, the correlation between Sherwood and Nusselt numbers is shown as [21,29]:

$$Sh=Nu\cdot\left(\frac{Sc}{Pr}\right)^{-1/3} \tag{7}$$

Due to the geometric and physical proprieties of the membrane (small thickness 100 μm, thermal conductivity…), the temperature difference between the two sides of a hydrophilic membrane is negligible. Some studies have shown that the temperature differences are in the order of 10^{-4} °C [30]. In addition, they proved that heat liberated on the fresh air side of the membrane could be absorbed by the exhaust air of the other side [31].

$$T_{m1}=T_{m2}=T_m \tag{8}$$

The sensible and latent effectiveness are defined by Eqs. (9) and (10):

$$\varepsilon_s=\frac{T_{fi}-T_{fo}}{T_{fi}-T_{ei}} \tag{9}$$

$$\varepsilon_l=\frac{\omega_{fi}-\omega_{fo}}{\omega_{fi}-\omega_{ei}} \tag{10}$$

3. Numerical approach

To solve the governing equations shown in the previous section, a computational fluid dynamics (CFD) is used. The PB MBHE geometrical details and properties are presented in Table 1.

The above equations (Eqs. (1)–(6)) are solved numerically using CFD code Fluent 6.3.26. The 2 DDP (2 Dimensions Double Precision) is chosen to resolve our two dimensional model. The Power Law scheme is used for discretizing the momentum and vapor water transport equations (it is adequate for low Reynolds numbers). In addition, the SIMPLE (Semi-Implicit Method for Pressure Linked Equations) algorithm is taken for pressure velocity coupling. The criterion of convergence for computational domain is ensured at different locations.

The PB MBHE geometry is designed and meshed using a grid package Gambit. The geometry including the two air channels and membrane surface are refined. In the *y*-direction a grid scale of $25 \cdot 10^{-6}$ m was selected for the two air channels and for the membrane surface, the grid scale increases to $25 \cdot 10^{-7}$ m while in the *x*-direction a similar grid scale of $5 \cdot 10^{-6}$ m was taken.

The associated boundary conditions are defined as follows:

Inlet conditions for the fresh air channel:

$$T_{in}=35\ ^\circ\text{C};\quad \omega_{in}=20\ \text{g kg}^{-1};\quad u_{in}=u_0;\quad v_{in}=0$$

Inlet conditions for the exhaust air channel:

$$T_{in}=25\ ^\circ\text{C};\quad \omega_{in}=10\ \text{g kg}^{-1};\quad u_{in}=u_0;\quad v_{in}=0$$

The PB MBHE core includes the external core and the different obstacles are considered to be adiabatic (wall):

$$\frac{\partial T}{\partial n}=0;\quad \frac{\partial \omega}{\partial n}=0$$

4. Model validation

In order to examine the numerical model of MBHE, a comparison with an experimental investigation of co-current MBHE is established. This experimentation carried out under inlet operating conditions: fresh air temperature 35 °C and fresh humidity ratio 20 g kg^{-1}, or 56.2% RH; exhaust air temperature 25 °C and exhaust humidity ratio 10 g kg^{-1}, or 50.6% RH. Generally, the thermal and mass diffusivities of membrane are affected by the temperature. For the considered operating conditions, they are considered constant and equal respectively to (λ_a = 0.0263 W m^{-1} K^{-1}), D_v = 2.62 - $\cdot 10^{-5}$ m^2 s^{-1}) [3].

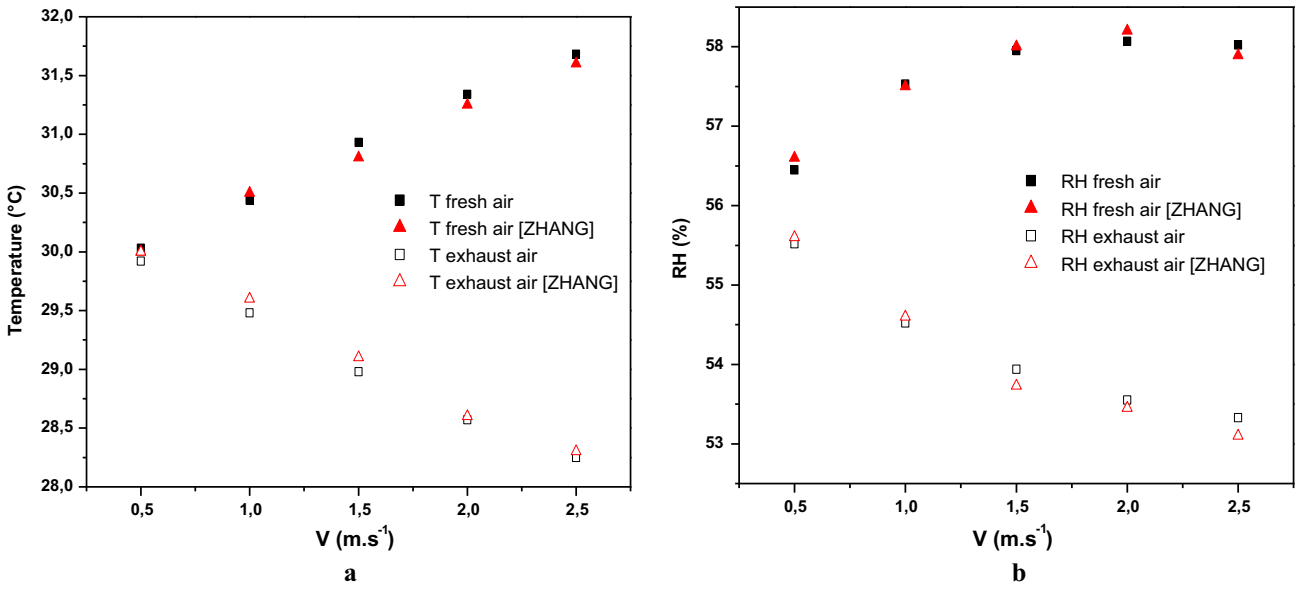

Fig. 2. Comparison between numerical and experimental: (a) temperature and (b) relative humidity values of fresh and exhaust air streams at outlet MBHE.

For the co-current flow arrangement, both fresh and exhaust air temperature and relative humidity (RH) values at outlet of MBHE are presented for several Reynolds number as shown in Fig. 2. The square points represent our numerical results; however the discrete triangle points represent the experimental measurements of Ref. [3]. By increasing the air velocity from 0.5 to 2.5 m s^{-1}, the temperature values increase linearly by 1.5 °C in the fresh air side while they decrease by 1.7 °C in the exhaust air side as plotted in Fig. 2a.

When the air velocity increases from 0.5 to 2.5 m s^{-1}, the RH values vary from 56.4% to 58% in the fresh air side, and decrease from 55.5% to 53% in the exhaust air side as depicted in Fig. 2b. The air velocity effect on the outlet air proprieties will be explained in the next section (Figs. 7 and 8).

The obtained numerical results are in agreement with the experimental data (Fig. 2). The difference percentages are within ±3%, which approved the consistency of the developed numerical model. This conformity allows us to investigate and to optimize a new MBHE geometry by changing the continuous air channels with partially blocked ones.

5. Simulation results and discussion

In order to denote the contribution of the new MBHE, Fig. 3 presents the outlet proprieties (temperature and humidity ratio) of both fresh and exhaust air streams for normal and partially blocked MBHE geometries, respectively.

At the inlet, the temperature and humidity ratio values of fresh and exhaust air streams are similar for both normal and PB geometries. However, the results show that the outlet values of temperature and humidity ratio to the PB geometry are lower than those of normal geometry MBHE as shown in Fig. 3a and b.

This signifies that the insertion of obstacles has a good influence on the heat and mass transfer rates. Although heat and mass transfer are increased through the membrane, the outlet temperature and humidity ratio values are also enhanced due to the obstacles effects in both fresh and exhaust air streams [32]. Therefore, the outlet air temperature and humidity ratio increase with decreasing Reynolds number.

As mentioned, the temperature distributions in membrane surfaces begin with different boundary conditions, however they finish with homogeneous values which prove by Eq. (8) as shown in Fig. 3a.

Generally, the geometry modification is usually used in air conditioning applications. These results confirm the efficiency of the PB MBHE and provide a solution to improve the heat and mass transfer rates in the membrane based technologies.

5.1. Obstacles number (n) impact

Following our previous suggestion, Fig. 4 shows the influence of obstacles number (n) on the outlet air proprieties under different air velocities. The obstacles number (n) is expressed as:

$$n = \frac{x_f}{b + c} \tag{11}$$

In order to appreciate the effects of obstacles number (n) on the heat and mass transfer rates, values of (n) changes from 4 to 9. As depicted from Fig. 4a, when the obstacles number (n) increases from 4 to 9, the temperature values at outlet fresh air side increase by 0.86 °C, while the outlet exhaust temperature values decrease by 0.73 °C. Further, the outlet humidity ratio values vary respectively by ±1.7 g kg^{-1} in fresh and exhaust air channels when (n) increases from 4 to 9 as can be seen in Fig. 4b.

These could explain that a closer or larger spacing causes higher changing of heat and transfer rates, as well as the outlet air proprieties in both fresh and exhaust channels. Therefore, the outlet air temperature and humidity ratio enhanced when the obstacles number (n) is lower.

As illustrated in Table 2, the obstacles number (n) has an impact on dimensionless numbers such as Nusselt number which decreases from 4.17 to 3.38 and Sherwood number which decreases from 4.01 to 3.25. However, these variations are small [15]. In addition, Nusselt number is generally higher than Sherwood number, because the thermal resistance is less than the mass resistance.

5.2. Obstacles form ratio (r) impact

In order to evaluate the influence of obstacle form (r) on the heat and mass transfer rates, the following parameter is defined as:

$$r = \frac{D_h}{a} \tag{12}$$

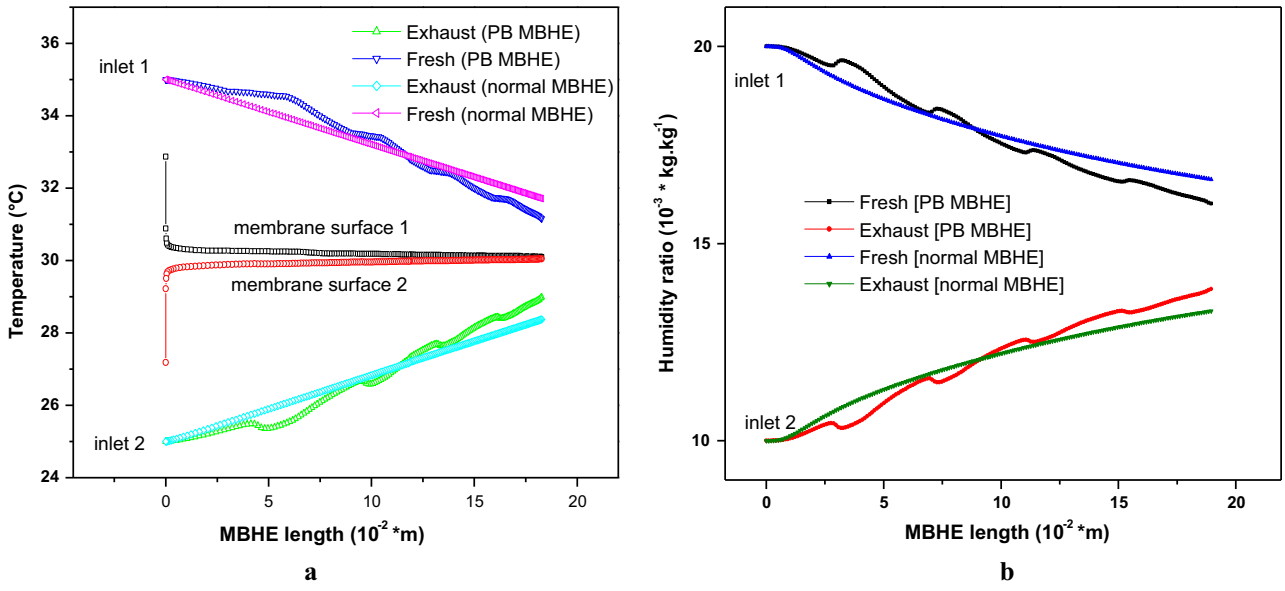

Fig. 3. (a) Temperature and b. humidity ratio distributions on the fresh and exhaust air channels in both normal and PB MBHE geometries.

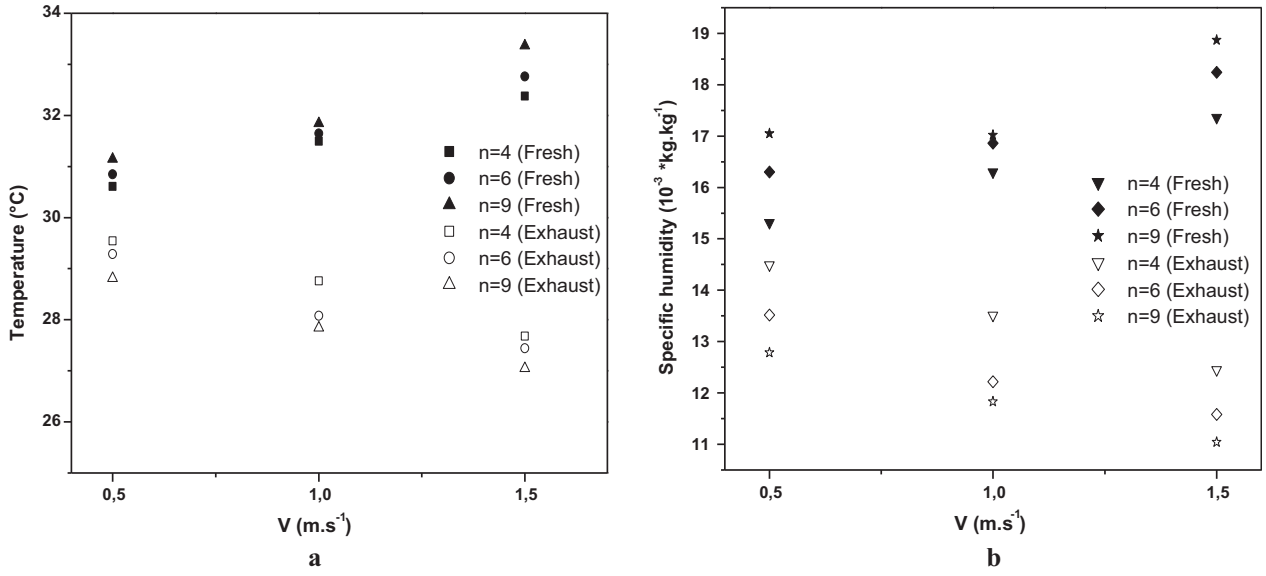

Fig. 4. Influence of obstacles number (n) on: (a) the fresh and exhaust air temperature and (b) fresh and exhaust air humidity ratio.

Table 2
Sherwood and Nusselt numbers under various obstacles number (n).

Normal ($n = 0$)		$n = 4$		$n = 6$		$n = 9$	
Nu	*Sh*	*Nu*	*Sh*	*Nu*	*Sh*	*Nu*	*Sh*
3.99	3.84	4.17	4.01	3.73	3.59	3.38	3.25

Fig. 5 shows the variations of air temperatures at the outlet fresh and exhaust sides with diverse PB forms ratio (r). As the obstacles form ratio (r) increases from 0.25 to 0.5, the air temperature at the outlet channel on the fresh side decreases while the temperature increases on the exhaust side.

Fig. 6 presents the air humidity ratio variations at the outlet fresh and exhaust sides for diverse PB forms ratio (r). A high obstacles form ratio (r) causes a strong variation on the specific humidity ratio which increases by 0.5 g kg^{-1} at the outlet exhaust air side, and decreases by 0.45 g kg^{-1} at the outlet fresh air side.

We can conclude from Figs. 5 and 6 that the air proprieties at outlet fresh and exhaust air sides vary adequately with the PB form ratio (r) which has a great effect on the mass and heat distributions between the two air sides of PB MBHE [33]. As indicated, when the obstacles form ratio (r) increases from 0.25 to 0.5, the Sherwood number decreases from 4.01 to 2.84, and the Nusselt number decreases from 4.17 to 2.95 as described in Table 3.

5.3. Inlet air velocity impact

Fig. 7 shows the influence of air velocities on the outlet fresh and exhaust air temperatures for velocity values ranging from 0.5 to 2 m s^{-1}. In this case, the Reynolds number changes from 124 to 496, and the regime of air flows is considered laminar. It can be seen in Fig. 7 that the temperature profiles for various air flow velocities are similar to significant variation on the outlet temperature values. By changing air velocities from 0.5 to 2 m s^{-1}, the air

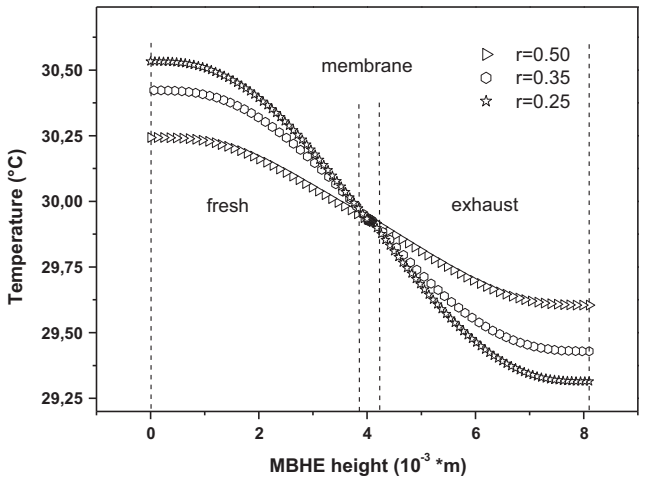

Fig. 5. Comparison between the PB form ratio (r) impact on fresh and exhaust air temperature values at outlet PB MBHE.

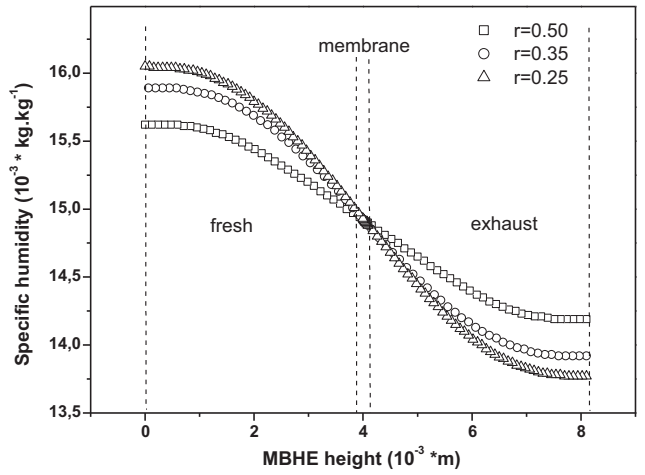

Fig. 6. Comparison between the PB form ratio (r) impact on fresh and exhaust air humidity ratio at outlet PB MBHE.

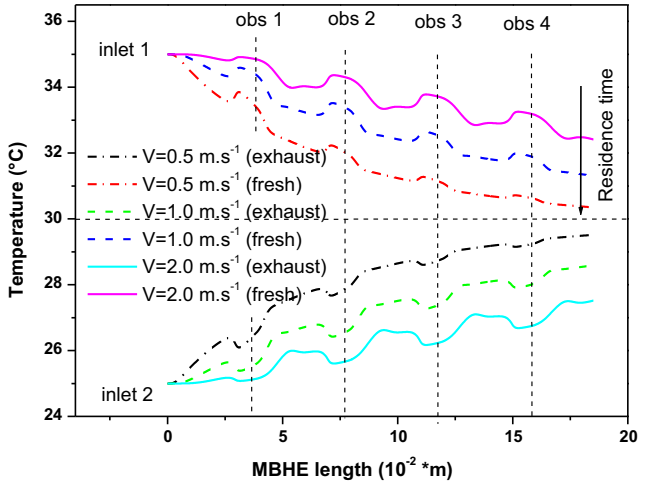

Fig. 7. Influence of air velocity values on the fresh and exhaust air temperature distributions ($n = 4$, $r = 0.25$).

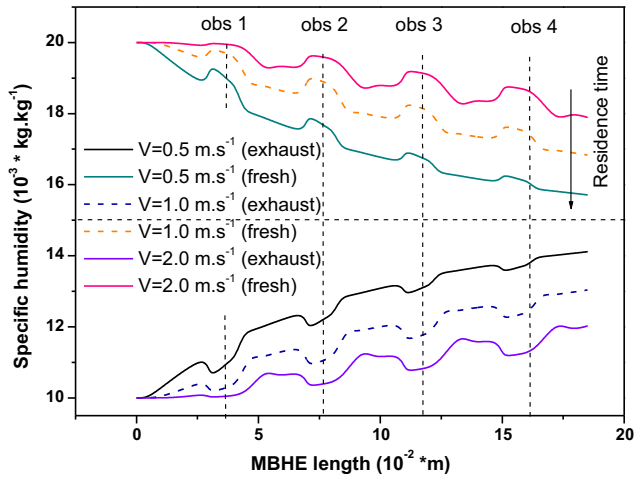

Fig. 8. Influence of air velocity values on the fresh and exhaust air humidity ratio distributions ($n = 4$, $r = 0.25$).

Table 3
Sherwood and Nusselt numbers under different obstacles form ratio (r).

$n = 4$, $r = 0.25$		$n = 4$, $r = 0.35$		$n = 4$, $r = 0.5$	
Nu	*Sh*	*Nu*	*Sh*	*Nu*	*Sh*
4.17	4.01	2.91	2.80	2.95	2.84

temperature values vary by 2 °C at outlet PB MBHE channels. Similarly to Fig. 7, Fig. 8 shows the influence of air velocities on the outlet humidity ratio in both fresh and exhaust sides. The outlet humidity ratio difference is equal to 3.78 g kg^{-1} when air velocities increase from 0.5 to 2 m s^{-1}. According to these results, a higher Reynolds number causes an increase (decrease) in the outlet air temperature and humidity ratio for the fresh and (exhaust) side. This indicates that the mass and heat transfer rates in the PB MBHE decreases under high air flow velocities [3]. It can also be observed in Figs. 7 and 8 that the residence time of air streams to exchange the heat and moisture through the hydrophilic membrane is very small in the high air velocities; however it becomes almost great at the low air velocities.

Sensible and latent effectiveness of co-current flow PB MBHE ($n = 4$, $r = 0.25$) are plotted in Fig. 9. As depicted, both sensible

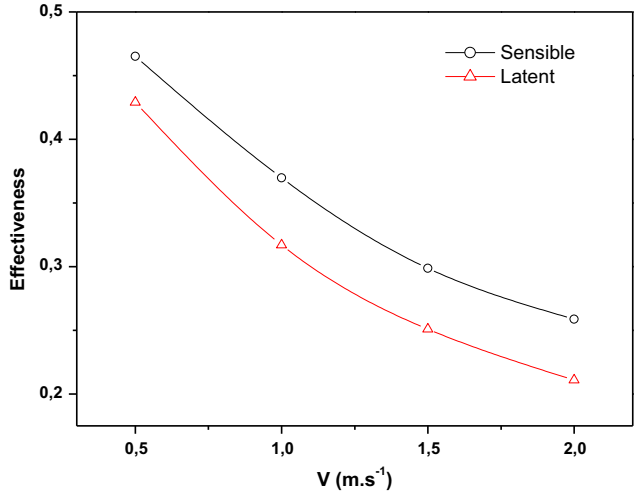

Fig. 9. Sensible and latent effectiveness of co current flow PB MBHE ($n = 4$, $r = 0.25$).

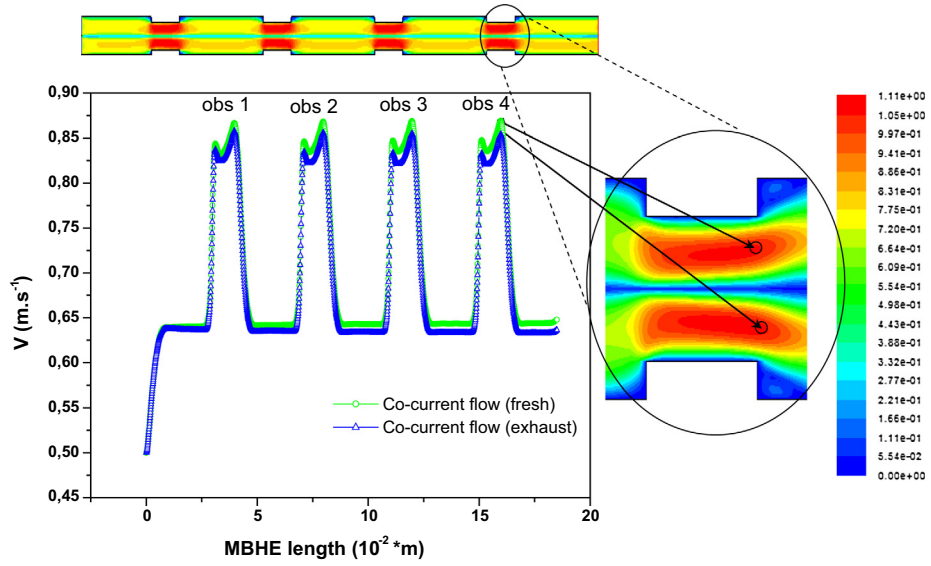

Fig. 10. Velocity distributions on the fresh and exhaust air channels of co-current flow PB MBHE.

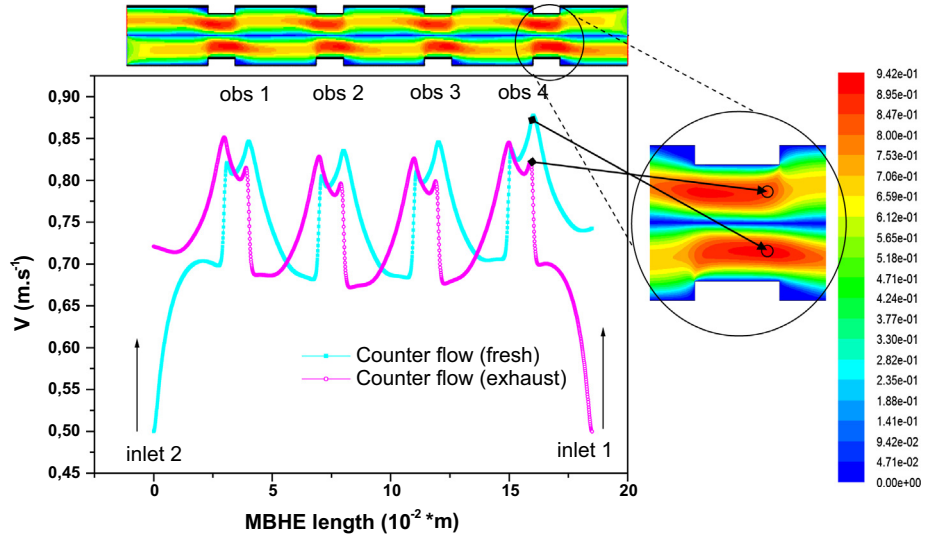

Fig. 11. Velocity distributions on the fresh and exhaust air channels of counter flow PB MBHE.

and latent effectiveness decrease simultaneously with increasing air flow velocity. The sensible effectiveness decreases from 4.65 to 2.58 while the latent effectiveness decreases from 4.29 to 2.11 with an increase in the air velocity from 0.5 to 2 m s^{-1}. This decrease may be explained by the better heat and mass transfer rates at low air flow velocities as shown in the previous figures.

5.4. PB MBHE geometry impact for different membrane materials

As can be seen in Table 4, the conductivity and diffusivity ratios for various used membranes in the total heat exchangers are presented. The raw data are taken from Refs. [2,34]. Since the mass transfer resistance is higher than the heat transfer resistance, the heat conductivity ratios are higher than mass diffusivity ratios. In

Table 4
Sherwood and Nusselt numbers under normal and PB MBHE with different membrane materials.

Membrane materials	λ_m (W m^{-1} K^{-1})	D_m (m^2 s^{-1})	$\tau_h = \frac{\lambda_m}{\lambda_a}$	$\tau_m = \frac{D_m}{D_v}$	Normal MBHE		PB MBHE (n = 4, r = 0.25)	
					Nu	*Sh*	*Nu*	*Sh*
PVA (polyvinylalcohol)	0.12	$2.5 \cdot 10^{-11}$	4.56	$9.54 \cdot 10^{-7}$	3.97	3.82	4.11	3.95
Modified PVA (used in our study)	0.13	$8 \cdot 10^{-6}$	4.94	3.05	3.99	3.84	4.17	4.01
PVC (polyvinyl chloride)	0.17	$1.67 \cdot 10^{-10}$	6.46	$6.37 \cdot 10^{-6}$	4.00	3.85	4.18	4.02
PDMS (polydimethylsiloxane)	0.23	$3.34 \cdot 10^{-8}$	8.74	$1.27 \cdot 10^{-3}$	4.02	3.86	4.22	4.05

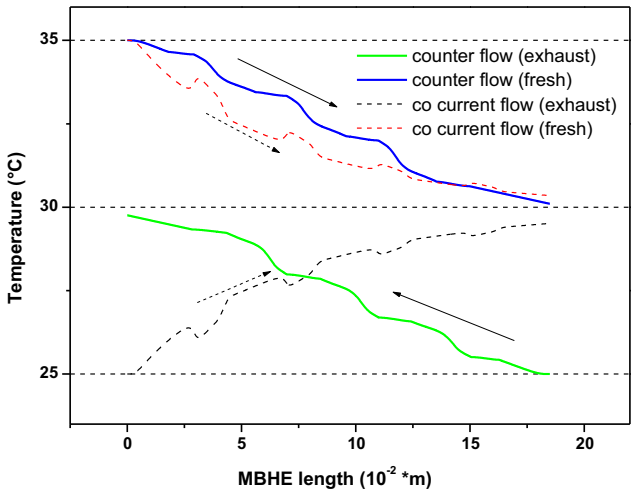

Fig. 12. Comparison between temperature values of co-current and counter flows of PB MBHE ($n = 4$, $r = 0.25$, $v = 0.5$ m s^{-1}).

addition, the lower heat conductivity (diffusivity) ratio causes greater temperature (humidity) gradients across membrane. Therefore, this is explained by the latent effectiveness which is generally lower than sensible one as shown in Fig. 9. This method of heat and mass transfer enhancement is established and used by researchers, so the literature on this topic is commonly apparent [35].

In the same Table 4, Nusselt and Sherwood numbers for normal and partially blocked MBHE geometries with various membrane proprieties are illustrated to discuss the membrane resistances effects on heat and mass transfer. As can be seen, the effects of membrane resistance are very small. The Nusselt and Sherwood numbers increases only by 0.05. Generally, the Sherwood numbers are less than Nusselt numbers, due to the different values of *Pr* and *Sc*. The MBHE geometry has also a little effect on Nusselt and Sherwood numbers. For example, the Nusselt and Sherwood numbers increase from 4.00 to 4.18 and from 3.85 to 4.02, respectively when we use the PVC (polyvinyl chloride). This signifies that both mass and heat transfer resistances are affected by membrane properties and operating conditions [36,37].

5.5. Flow arrangement impact

The distribution of air velocity for co current flow PB MBHE is shown in Fig. 10. At the top surface of obstacles, the velocity values increase 25% much more than the mean values in the center of the air channels. At the fresh and exhaust channels, Fig. 10 shows symmetric profiles of the air velocity distributions due to similar boundary and design conditions of PB MBHE ($v = 0.5$ m s^{-1}, $n = 4$, $r = 0.25$). In addition, the velocity values decrease progressively to achieve zero near the membrane. At the internal walls of solid layer, the velocity distributions show null values in the fresh and exhaust air sides with a fluid recirculation near the obstacles [33].

The air velocity distributions for counter flow PB MBHE are observed in Fig. 11. By comparing with Fig. 10, the velocity values increase at the top of obstacle surfaces and decrease progressively near the regions adjacent to the hydrophilic membrane and internal walls of solid layer. However, the profile of air velocity at the fresh and exhaust sides is inversed due to counter flow arrangement as shown in Fig. 11.

The impact of flow arrangements on the outlet fresh and exhaust air temperatures is plotted in Fig. 12 at similar conditions ($v = 0.5$ m s^{-1}, $n = 4$, $r = 0.25$). We remark that for both flow arrangements, the temperature decreases (increases) at the fresh (exhaust) channel. However, the outlet values decrease more rapidly for counter than co-current flows PB MBHE. Apart from these cases, counter flow arrangement offers the best exchange than co-current flow arrangement [3,21].

6. Conclusion

A novel membrane based heat exchanger is numerically investigated. The momentum, energy and mass transport equations are developed to describe the hydrodynamic, heat and mass transfer in the considered MBHE. The good agreement between our numerical results and experimental data allowed us to study the obstacles effects on the heat and mass transfer rates. Therefore, the following results have been established:

- The existence of obstacles in the MBHE design enhances both heat and mass transfer rates between fresh and exhaust air channels.
- A low obstacles number (n) leads to a large (small) air temperature and specific humidity values in the exhaust (fresh) air channel.
- Obstacle form ratio (r) has a strong effect on the temperature and humidity distributions when it becomes higher.
- Membrane proprieties in the PB MBHE geometry have a strong effect on the Nusselt and Sherwood numbers.
- By varying the flow arrangement, the velocity distributions in the fresh and exhaust air channels are changed. Also, the outlet temperature values are higher for counter more than co-current flow arrangements.

A research project, in progress, carries to fabricate novel MBHEs with various membranes in order to compare and to validate this numerical results under diverse operating conditions.

References

[1] R. Sebai, R. Chouikh, A. Guizani, Cross-flow membrane-based enthalpy exchanger balanced and unbalanced flow, Energy Convers. Manage. 87 (2014) 19–28.
[2] L.Z. Zhang, Y.Y. Wang, C.L. Wang, H. Xiang, Synthesis and characterization of a PVA/LiCl blend membrane for air dehumidification, J. Membr. Sci. 308 (1–2) (2008) 198–206.
[3] L.Z. Zhang, C.H. Liang, L.X. Pei, Conjugate heat and mass transfer in membrane-formed channels in all entry regions, Int. J. Heat Mass Transf. 53 (2010) 815–824.
[4] R. Al-Waked, M.S. Nasif, G. Morrison, M. Behnia, CFD simulation of air to air enthalpy heat exchanger, Energy Convers. Manage. 74 (2013) 377–385.
[5] P. Wais, Influence of fin thickness and winglet orientation on mass and thermal efficiency of cross-flow heat exchanger, Appl. Therm. Eng. 102 (2016) 184–195.
[6] J.C. Min, M. Su, Performance analysis of a membrane-based enthalpy exchanger: effects of the membrane properties on the exchanger performance, J. Membr. Sci. 348 (1) (2010) 376–382.
[7] J.C. Min, M. Su, Performance analysis of a membrane-based energy recovery ventilator: effects of membrane spacing and thickness on the ventilator performance, Appl. Therm. Eng. 30 (8) (2010) 991–997.
[8] J. Woods, E. Kozubal, Heat transfer and pressure drop in spacer-filled channels for membrane energy recovery ventilators, Appl. Therm. Eng. 50 (1) (2013) 868–876.
[9] X.H. Ye, M.D. Levan, Water transport properties of Nafion membranes: Part I. Single-tube membrane module for air drying, J. Membr. Sci. 221 (2003) 147–161.
[10] Z.M. Wan, J.H. Wan, J. Liu, Z.K. Tu, M. Pan, Z.C. Liu, W. Liu, Water recovery and air humidification by condensing the moisture in the outlet gas of a proton exchange membrane fuel cell stack, Appl. Therm. Eng. 42 (2012) 173–178.
[11] A.A. Al-Farayedhi, P. Gandhidasan, S.Y. Ahmed, Regeneration of liquid desiccants using membrane technology, Energy Convers. Manage. 40 (1999) 1405–1411.
[12] L. Dilandro, M. Pegoraro, L. Bordogna, Interaction of polyether-polyurethane with water vapor and water–methane separation selectivity, J. Membr. Sci. 64 (1991) 229–236.
[13] P. Scovazzo, A. Hoehn, P. Todd, Membrane porosity and hydrophilic membrane based dehumidification performance, J. Membr. Sci. 167 (2000) 217–225.

[14] J. Zhao, B. Li, X. Li, Y. Qin, C. Li, S. Wang, Numerical simulation of novel polypropylene hollow fiber heat exchanger and analysis of its characteristics, Appl. Therm. Eng. 59 (2013) 134–141.
[15] S.M. Huang, F.G.F. Qin, M. Yang, X. Yang, W.F. Zhong, Heat and mass transfer deteriorations in an elliptical hollow fiber membrane tube bank for liquid desiccant air dehumidification, Appl. Therm. Eng. 57 (2013) 90–98.
[16] P. Aranda, W.J. Chen, C.R. Martin, Water transport across polystyrenesulfonate/alumina composite membranes, J. Membr. Sci. 99 (1995) 185–195.
[17] J. Min, M. Su, Performance analysis of a membrane-based enthalpy exchanger: effects of the membrane properties on the exchanger performance, J. Membr. Sci. 348 (2010) 376–382.
[18] J. Min, J. Duan, Membrane-type total heat exchanger performance with heat and moisture transferring in different directions across membranes, Appl. Therm. Eng. 91 (2015) 1040–1047.
[19] S. Chung, C.D. Seo, H. Lee, J.H. Choi, J. Chung, Design strategy for networking membrane module and heat exchanger for direct contact membrane distillation process in seawater desalination, Desalination 349 (2014) 126–135.
[20] D.G. Moghaddam, P. LePoudre, G. Ge, R.W. Besant, C.J. Simonson, Small-scale single-panel liquid-to-air membrane energy exchanger (LAMEE) test facility development, commissioning and evaluating the steady-state performance, Energy Build. 66 (2013) 424–436.
[21] L.Z. Zhang, Heat and mass transfer in a quasi-counter flow membrane-based total heat exchanger, Int. J. Heat Mass Transf. 53 (2010) 5478–5486.
[22] H. Yu, X. Yang, R. Wang, A.G. Fane, Numerical simulation of heat and mass transfer in direct membrane distillation in a hollow fiber module with laminar flow, J. Membr. Sci. 384 (2011) 107–116.
[23] W.X. Li, T.S. Zhong, J.L. Niu, L.Z. Zhang, Conjugate heat and mass transfer in a total heat exchanger with cross-corrugated triangular ducts and step made asymmetric membranes, Int. J. Heat Mass Transf. 84 (2015) 390–400.
[24] L.Z. Zhang, F. Xiao, Simultaneous heat and moisture transfer through a composite supported liquid membrane, Int. J. Heat Mass Transf. 51 (2008) 2179–2189.
[25] X.R. Zhang, L.Z. Zhang, H.M. Liu, L.X. Pei, One-step fabrication and analysis of an asymmetric cellulose acetate membrane for heat and moisture recovery, J. Membr. Sci. 366 (2011) 158–165.
[26] L.Z. Zhang, Progress on heat and moisture recovery with membranes: from fundamentals to engineering applications, Energy Convers. Manage. 63 (2012) 173–195.
[27] P.W. Majsztrik, M.B. Satterfield, A.B. Bocarsly, J.B. Benziger, Water sorption, desorption and transport in Nafion membranes, J. Membr. Sci. 301 (2007) 93–106.
[28] L.Z. Zhang, Heat and mass transfer in a cross-flow membrane-based enthalpy exchanger under naturally formed boundary conditions, Int. J. Heat Mass Transf. 50 (2007) 151–162.
[29] F.P. Incropera, D.P. Dewitt, T.L. Bergman, A.S. Lavine, Fundamentals of Heat and Mass Transfer, sixth ed., 2007 (pp. 378, Chapter 6).
[30] L.Z. Zhang, Y. Jiang, Y.P. Zhang, Membrane-based humidity pump: performance and limitations, J. Membr. Sci. 171 (2000) 207–216.
[31] E. Favre, Temperature polarization in pervaporation, Desalination 154 (2003) 129–138.
[32] S. Sripattanapipat, P. Promvonge, Numerical analysis of laminar heat transfer in a channel with diamond-shaped baffles, Int. J. Heat Mass Transf. 36 (2009) 32–38.
[33] M. Shakaib, S.M.F. Hasani, M. Mahmood, CFD modeling for flow and mass transfer in spacer-obstructed membrane feed channels, J. Membr. Sci. 326 (2009) 270–284.
[34] H. Sijbesma, K. Nymeijer, R. van Marwijk, R. Heijboer, J. Potreck, M. Wessling, Flue gas dehydration using polymer membranes, J. Membr. Sci. 313 (2008) 263–276.
[35] L.Z. Zhang, Heat and mass transfer in plate-fin enthalpy exchangers with different plate and fin materials, Int. J. Heat Mass Transf. 52 (11–12) (2009) 2704–2713.
[36] J. Min, M. Su, Performance analysis of a membrane-based energy recovery ventilator: effects of outdoor air state, Appl. Therm. Eng. 31 (2011) 4036–4043.
[37] Z.X. Li, T.S. Zhong, J.L. Niu, F. Xiao, L.Z. Zhang, Conjugate heat and mass transfer in a total heat exchanger with cross-corrugated triangular ducts and one-step made asymmetric membranes, Int. J. Heat Mass Transf. 84 (2015) 390–400.